Journal of the Mechanical Behavior of Biomedical Materials 98 (2019) 96–107

Contents lists available at ScienceDirect

Journal of the Mechanical Behavior of Biomedical Materials

journal homepage: www.elsevier.com/locate/jmbbm

A micromechanical model for the growth of collagenous tissues under mechanics-mediated collagen deposition and degradation

Zheng Jia[a,b], Thao D. Nguyen[b,*]

[a] Department of Engineering Mechanics, Key Laboratory of Soft Machines and Smart Devices of Zhejiang Province, Zhejiang University, Hangzhou, 310027, China
[b] Department of Mechanical Engineering, Johns Hopkins University, 3400 N. Charles St., Baltimore, MD, 21218, USA

ARTICLE INFO

Keywords:
Growth
Collagen deposition
Degradation
Homeostasis
Stress

ABSTRACT

In this study, we developed a micromechanical model for the growth and remodeling of a soft tissue based on the concurrent action of collagen deposition and degradation. We assumed in the model that collagen degradation causes a reduction in the fiber radius, while collagen deposition can increase both the radius and length of the collagen fibers growing under load. The latter arises from the assumption that collagen is deposited in an unstressed state, which increases the reference length of a fiber growing under mechanical load. The rate of collagen deposition and degradation can be stimulated and inhibited, respectively, by the fiber axial strain energy density. From these assumptions, we derived kinetic relationships for the fiber radial and axial growth stretch, and constitutive relations for the stress response and growth and remodeling of the tissues. We applied the model to study the growth of collagen fibers under a static and cyclic force. Cyclic force loading can drive the continual axial growth of collagen fiber, while the axial growth under a constant force eventually halts when an equilibrium state is reached. We then applied the model to investigate the development of stress and strain homeostasis of a spherical collagenous tissue membrane in response to a perturbation in the internal pressure. The model showed that an increase in the pressure produced growth in the tissue radius and thickness, such that the stress response was able to recover the equilibrium membrane stress before the pressure perturbation. Tissues composed of slender, or low-crimp collagen fibers also recovered the equilibrium mechanical stretch level before the perturbation. These results indicated that concurrent mechanics-stimulated collagen deposition and mechanics-inhibited degradation can produce stress homeostasis and for some fiber morphology strain homeostasis without prescribing a target stress or fiber strain.

1. Introduction

Soft collagenous tissues exhibit a highly organized microstructure of collagen and elastin fibers arranged in a soft hydrated matrix of cells, proteoglycans and other non-fiber forming proteins. The collagen fibers exhibit a crimped (wavy) morphology in an unloaded state. The degree of fiber alignment and fiber crimp are tailored to the mechanical function of the tissue. Collagen fibers in tendon have a high degree of crimp and alignment to enable high deformability at low levels of strains and high stiffness (low deformability) at high levels of strain to enable the range of daily motion (Brown, 1972). The collagen structure of the central cornea and posterior sclera, away from the limbus and peripapillary regions, feature an isotropic arrangement of stiff fibers with low crimp, to minimize deformation from daily fluctuations in the intraocular pressure and maintain a stable shape for light refraction (Boote et al., 2008; Nguyen and Boyce, 2011; Young, 1985).

The structure of soft tissues are not static but are actively maintained and changed by the process of growth and remodeling (Prajapati et al., 2000). Growth refers to an increase in mass, which can manifest as an increase in volume or density, while remodeling refers to a change in material properties caused by changes in the extracellular matrix microstructure. Growth and remodeling in soft tissues can occur in response to a prolonged change in mechanical loading. Collagen formation and degradation increase immediately after exercise in human bodies and a net collagen synthesis is found 36–72 h after exercise (Magnusson et al., 2010). A chronic increase in the intraocular pressure in mouse models of glaucoma causes the sclera to expand and thin or thicken depending on the scleral region (Nguyen et al., 2013), the collagen fiber arrangement to become more isotropic (Pijanka et al., 2015), and the stress-strain response to stiffen (Nguyen et al., 2013). In addition, two-thirds of the astronauts suffer from hyperopia after extended missions in the International Space Station, because the micro-

* Corresponding author.
E-mail address: vicky.nguyen@jhu.edu (T.D. Nguyen).

https://doi.org/10.1016/j.jmbbm.2019.06.004
Received 25 February 2019; Received in revised form 30 May 2019; Accepted 5 June 2019
Available online 07 June 2019
1751-6161/

gravity environment leads to an elevated intracranial pressure, which shortens and flattens the back of the sclera (Alperin and Bagci, 2018). For many tissues growth and remodeling has the effect of restoring a preferred tissue stress or strain state, a process referred to as homeostasis. The concept of a homeostatic stress state has been applied successfully to describe growth of arteries in response to changes in the wall shear and membrane stresses (Cyron and Humphrey, 2014; Humphrey and Rajagopal, 2002; Taber, 1998; Taber and Humphrey, 2001), hypertrophic growth of the left ventricle caused by pressure overload (Kerckhoffs, 2012; Rodriguez et al., 1994), growth and remodeling of aneurysms (Baek et al., 2006; Cyron et al., 2016; Humphrey and Holzapfel, 2012), and tendons and ligaments (Cyron and Humphrey, 2017). However, growth and remodeling can proceed unstably in many diseases involving fibrosis and tissue degeneration, such as osteoarthritis.

Growth and remodeling have been treated traditionally in theoretical models as distinct phenomena (Menzel and Kuhl, 2012). However, more recent micromechanical modeling approaches have recognized that they likely occur together through continuous deposition and degradation of collagen and other tissue components under load. Mechanical loading can affect the rate of deposition and degradation through active cellular mechanisms and passive chemo-mechanical mechanisms. Mechanical loading can enhance the active contraction of fibroblasts and stimulate the production of matrix metalloproteinases (Adhikari et al., 2011), tissue inhibitors of matrix metalloproteinases, collagen and other extracellular matrix products (Chiquet et al., 2003; Li et al., 1998). Mechanical stretch can also alter the degradation rate of collagen and elastin. Numerous studies have shown that mechanical stretch can decrease the rate of enzymatic degradation of collagen molecules, collagen fibrils, reconstituted collagen fiber networks and decellularized collagen constructs in bacterial collagenase (Bhole et al., 2009; Flynn et al., 2010; Huang and Yannas, 1977; Ruberti and Hallab, 2005; Zareian et al., 2010). Furthermore, enzymatic degradation of tissue becomes minimum or is halted at the transition stretch marking the initiation of rapid stiffening in the stress-strain curve of the tissue (Huang and Yannas, 1977; Zareian et al., 2010).

We previously developed a theoretical micromechanical model of fibrous collagen tissues to examine the effects of mechanical inhibition of enzymatic degradation on the remodeling of collagen networks (Tonge et al., 2015). The model was developed based on the central hypotheses that enzymatic degradation of collagen fibers is an energy-activated process and that the activation energy is increased by the axial strain energy density of the collagen fibers. We assumed that the collagen fibers are initially crimped and respond to mechanical force by unbending (straightening) then stretching axially. Furthermore, enzymatic degradation acts to decrease the radius of the collagen fibers. The parameters of the energy-activated degradation law were fit to fibril-level degradation experiments and the model was applied successfully to predict the effects of mechanical loading observed in tissue-level degradation experiments. Specifically, the model predicted that wavy collagen fibers of a tissue under tension are degraded until they straighten, such that tissue degradation is halted when the stretch reached the transition stretch of the tissue stress-strain curve. The morphology of the collagen fibers influenced the rate of tissue-degradation. Tissues with less crimped and slender fibers, which straightened at lower strains levels, were more resistant to enzymatic degradation. Mechanical inhibition of enzymatic degradation caused the anisotropic fiber arrangement to remodel along the direction of the maximum principal stress. Furthermore, the degree of anisotropy depends on the state of stress. An initially isotropic collagen network undergoing enzymatic degradation remodeled towards a highly aligned anisotropic structure under uniaxial tension but remained an isotropic network under equibiaxial tension. These findings showed that mechanical inhibition of enzymatic degradation may play an important role in tailoring the collagen crimp morphology and anisotropic structure to the physiological loading state of the tissue.

The goal of this work was to develop a model for tissue growth and remodeling by combining the micro-mechanisms of mechanical inhibition of collagen degradation and mechanical stimulation of collagen deposition and investigate their effects on the development of stress homeostasis. Previous works have incorporated these micro-mechanisms to investigate various aspects of the remodeling of collagen networks (Demirkoparan et al., 2013; Gyoneva et al., 2016; Hadi et al., 2012; Topol et al., 2014, 2017). Heck et al. (2015) and Loerakker et al. (2014) also incorporated the effects of cellular traction tugging on collagen fibers to describe the remodeling of the transition strain of stress-strain response caused by the shortening or lengthening of the embryonic periosteum strips (Foolen et al., 2010) and the reorientation of collagen fibers in engineered tissue strips under load (Jhun et al., 2009; Sander et al., 2011). The deposition of collagen in a tissue under load can alter the natural configuration of the collagen fibers and produce growth along the fiber plane if the collagen is deposited at different stress level than the fiber stress. This process is widely represented in micromechanical models by the evolution of the collagen fiber growth stretch or an analogous quantity to denote the changing reference length of the fiber. Growth and remodeling attains a material equilibrium when the rate of degradation equals the rate of deposition. However, the growth and remodeling equilibrium adapts to the changing mechanical loading and does not in general recover a homeostatic target (Gyoneva et al., 2016). To realize homeostasis, various models have prescribed a target stress (Cyron et al., 2016; Rausch et al., 2011; Taber and Humphrey, 2001), established for example by contracting fibroblasts, to drive the evolution of the fiber growth stretch. Another approach evolves the fiber growth stretch towards a target stretch, which can represent the stretch at which cells deposit collagen onto fibrils (Watton et al., 2009) or the fiber stretch corresponding to the stress exerted by contracting fibroblasts (Loerakker et al., 2014).

In this work, we investigated whether stress or strain homeostasis can arise in a collagen fiber network from the underlying micro-mechanisms of mechanical inhibition of collagen degradation, mechanical stimulation of deposition, and the evolution of the fiber growth stretch for a tissue under load without a prescribed homeostatic target. Collagen degradation is assumed to decrease the fiber radius of crimp fibers, while deposition increases the fiber radius according to a zeroth order, energy-activated kinetic relation. Mechanical stimulation of collagen production is represented in the model by the assumption that the deposition rate increases with the axial strain energy of the collagen fiber. We further assumed that collagen is deposited onto the fiber in an unstressed state and derived an evolution equation for the axial growth stretch of the fiber by considering the redistribution of the fiber stress upon unloading. The model was applied to examine the growth of a crimped collagen fiber subjected to a static and cyclic force and the growth and remodeling of spherical collagen membrane caused by perturbations in the internal pressure. The membrane example was motivated by the experiments of Brown et al. (Brown et al. (1998) and Ezra et al. (2010), which cultured fibroblasts in a collagen gel strips and measured the tension generated by cellular contraction of the gel in response to changes in the applied loading. The experiments showed that cells responded to perturbations in the applied loading by changing the matrix stress in the opposite direction of the applied load to restore the value before the perturbation. The model was able to predict the development of a homeostatic equibiaxial stress state, in which the growth and remodeling processes acted in response to a perturbation in the applied pressure to restore the membrane stress to the value prior to the perturbation. Furthermore, the homeostatic state depended on the degradation and deposition parameters and the material properties and crimp morphology of the collagen fibers. These findings provide new insights into the underlying mechanisms of mechanical homeostasis and the effect of fiber morphology and properties on homeostasis.

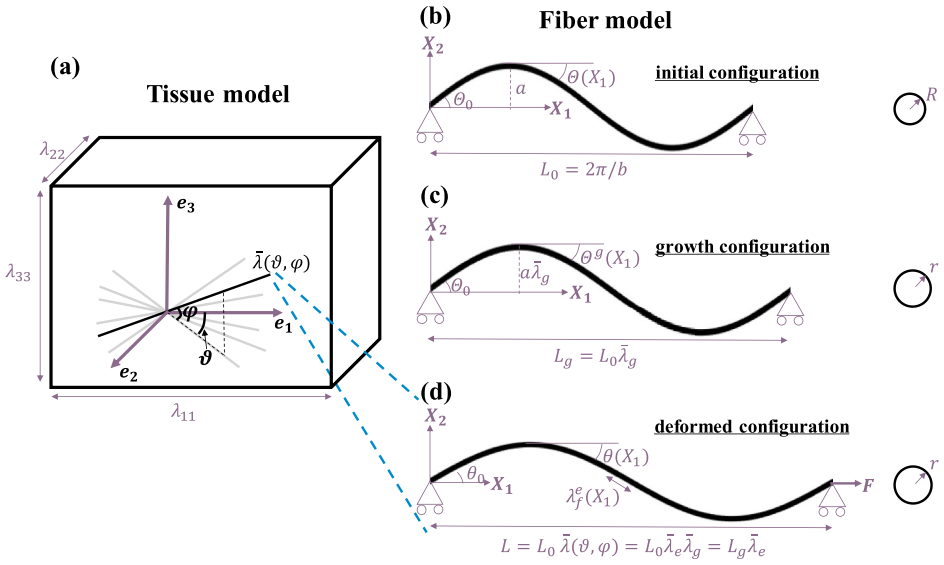

Fig. 1. (a) Schematic of collagenous tissues represented as a 3D distribution of wavy fibers. The tissue-level deformation imposes a macroscopic stretch $\bar{\lambda}(\vartheta, \phi)$ to each fiber. The wavy fiber morphology in the initial, growth, and current configurations are given in (b), (c), and (d), respectively.

2. Micro-mechanical model of collagenous tissues

In this section, we formulate a micro-mechanical model for collagenous tissues subjected to concurrent collagen deposition and degradation under load, by integrating a fiber-level growth law into a hyperelastic, distributed fiber tissue model.

2.1. Nonlinear mechanical response of collagen fibers

We develop a nonlinear mechanical model of a wavy collagen fiber on the basis of the elastica model developed by Comninou and Yannas (1976). As shown in Fig. 1, the wavy fiber is taken to be a planar sinusoidal beam with a circular cross section of initial radius R. In the initial configuration, the shape of the fiber is prescribed by $X_2 = a\sin(bX_1)$, where X_1 and X_2 are the coordinates along the horizontal and vertical directions in the local coordinate system of the fiber, a is the crimp amplitude, and b specifies the crimp period, which is related to the length of the wavy fiber projected onto the horizontal axis by $L_0 = 2\pi/b$. Assuming that the crimp angle is small, the rotation angle of the wavy fiber in the undeformed configuration is $\Theta(X_1) \approx \frac{dX_2}{dX_1} = ab\cos(bX_1) = \Theta_0\cos(bX_1)$. The $\Theta_0 = ab$ denotes the initial crimp angle, defined as the rotation angle at $X_1 = 0$.

In the presence of collagen monomers and collagenase, collagen deposition works in concert with enzymatic degradation to drive the growth of collagen fibers, leading to alterations in both fiber radius and length. Motivated by the experimental observations of Foolen et al. (2010), we assume that the growth process changes the fiber length by a factor of $\bar{\lambda}_g$, i.e., the axial growth stretch ratio, but does not affect the fiber crimp angle. This assumption is in line with the experimental evidence reported by Foolen et al. (2010). Therefore, in the stress-free growth configuration, a material element located at coordinates (X_1, X_2) in the initial configuration moves to (X_1^g, X_2^g), where $X_1^g = \bar{\lambda}_g X_1$ and $X_2^g = \bar{\lambda}_g X_2$. The wavy fiber shape in the growth configuration is given by $X_2^g = a\bar{\lambda}_g \sin\left(\frac{bX_1^g}{\bar{\lambda}_g}\right)$. Thus the projected length and amplitude of the wavy fiber in the growth configuration are given by the fiber growth stretch $L_g = \frac{2\pi\bar{\lambda}_g}{b} = L_0\bar{\lambda}_g$ and $a_g = a\bar{\lambda}_g$. With these assumptions, the rotation angle becomes $\Theta^g(X_1) = \Theta_0\cos\left(\frac{bX_1^g}{\bar{\lambda}_g}\right)$, and the crimp angle remains $\Theta_0 = ab$. The change in the fiber radius from R to r is represented by the radial growth ratio $D = r/R$ that is independent from the fiber growth stretch $\bar{\lambda}_g$.

The following assumptions are made to derive an analytical model for the mechanical response of the wavy fiber to an applied force (Comninou and Yannas, 1976; Tonge et al., 2015). (1) The collagen fiber is overall stress-free in an intermediate growth configuration, such that the growth configuration can be adopted as the reference state to define strain energy density and calculate fiber force. (2) The collagen fiber itself is taken to be linearly elastic with Young's modulus E. Therefore, the nonlinear mechanical response of collagen fibers arises from the wavy geometry. (3) The axial fiber strain is small, such that the Poisson's effect of deformation on fiber radius is negligible. Thus, a change in the radial growth ratio D occurs only from collagen deposition and degradation. (4) The radius of the wavy fiber is small compared to the fiber length, such that the straightening response can be described by Euler beam bending theory with negligible shear stresses. For a wavy collagen fiber simply supported at $X_1 = 0$ and subjected to a horizontal tensile force F at $X_1 = L_g$ (Fig. 1), the deformed rotation angle θ, fiber elastic axial stretch λ_f^e, and the macroscopic fiber stretch $\bar{\lambda} = L_0/L$ can be solved using the assumptions of Euler bending and small crimp angle as,

$$\theta(\bar{X}_1) = \frac{\beta}{\alpha(1+\alpha)+\beta}\Theta^g(\bar{X}_1), \tag{1}$$

$$\lambda_f^e(\bar{X}_1) = 1 + \alpha\cos(\theta(\bar{X}_1)), \tag{2}$$

$$\bar{\lambda} = \bar{\lambda}_g\int_0^1 \lambda_f^e(\bar{X}_1)\frac{\cos(\theta(\bar{X}_1))}{\cos(\Theta^g(\bar{X}_1))}d\bar{X}_1 \tag{3}$$

where $\alpha = F/EA$ is a normalized fiber force, $A = \pi r^2$ is the fiber area, and $\beta = \frac{b^2r^2}{4\bar{\lambda}_g^2} = \frac{b^2R^2}{4}\frac{D^2}{\bar{\lambda}_g^2} = \beta_0\frac{D^2}{\bar{\lambda}_g^2}$ is the fiber slenderness ratio in the deformed configuration. The slenderness ratio is a geometric factor that along with the fiber modulus E determines the bending stiffness of the fiber. $\bar{X}_1$ is the normalized coordinates defined as $\frac{X_1^g}{L_g}$. By prescribing a macro-stretch $\bar{\lambda}$, the normalized fiber force α can be solved numerically from Eqs. (1)–(3).

The strain energy density W_f of the deformed collagen fiber can be defined as the total strain energy divided by the fiber volume in the growth configuration. The total strain energy consists of two parts: the bending energy associated with straightening the wavy fiber and the axial strain energy corresponding to axially stretching the fiber. More detailed developments can be found in Section A of the Supporting Information. The strain energy density W_f can be expressed as

$$W_f = \int_0^1 \frac{E\beta}{2}[\theta(\bar{X}_1) - \Theta^g(\bar{X}_1)]^2 d\bar{X}_1 + \int_0^1 \frac{E}{2}[\lambda_f^e(\bar{X}_1) - 1]^2 d\bar{X}_1, \tag{4}$$

where the first term represents the bending strain energy, $W_{bending}$, and the second term is the axial strain energy density, W_{axial}. The $\theta(\bar{X}_1)$ and $\lambda_f^e(\bar{X}_1)$ are affected by the growth of collagen fiber through the fiber force α and the fiber slenderness ratio β in Eqs. (1) and (2).

2.2. Growth model of collagen fibers

We assumed that collagen deposition occurs through the process in which collagen monomers generated by fibroblasts bind to the collagen fiber surface, thereby increasing the fiber radius; while collagen degradation proceeds by removing collagen at the fiber surface in the presence of collagenase, which reduces the fiber radius. To describe the effects of mechanical inhibition of the enzymatic degradation of collagen (Flynn et al., 2010) and mechanical stimulation of cells leading to collagen production (Gyoneva et al., 2016), we assumed that the axial strain energy density W_{axial} acts to decrease the collagen degradation rate k_{deg} and increase deposition rate k_{dep} as follows,

$$k_{deg}(t) = G_1 \exp\left(-\frac{W_{axial}}{G_2}\right), \quad k_{dep}(t) = G_3 \exp\left(\frac{W_{axial}}{G_4}\right), \tag{5}$$

where G_3 and G_1 are the deposition and degradation rate of the unloaded fiber, and G_4 and G_2 are the activation energies for mechanical enhancement and inhibition relatively. The effects of the bending strain energy are not included in Eq. (5), because the bending of collagen fiber gives rise to a strain gradient across the fiber diameter, which would result in heterogeneous degradation and deposition rates along the fiber. Assuming that both degradation and deposition are zeroth order kinetic processes, the radial growth rate can be formulated as the competition between the deposition and degradation rate,

$$\frac{dD(t)}{dt} = k_{dep}(t) - k_{deg}(t) = G_3 \exp\left(\frac{W_{axial}}{G_4}\right) - G_1 \exp\left(-\frac{W_{axial}}{G_2}\right), \tag{6}$$

We assumed that collagen is deposited in an unstressed state. Thus, a collagen deposition onto a stressed fiber alters the reference length of the fiber, which at time t is denoted by $L_g(t) = L_0\bar{\lambda}_g(t)$. To derive an evolution equation for the growth fiber stretch, we consider the case of a net deposition, $k_{dep}(t) - k_{deg}(t) > 0$, onto a fiber subjected to a macroscopic $\bar{\lambda}(t)$. The deformed length of the fiber along X_1 at time t is given by, $L(t) = L_0\bar{\lambda}(t)$ and the reference length is $L_g(t) = L_0\bar{\lambda}_g(t)$ (Fig. 2). At time $t + dt$, a new layer of collagen (highlighted in red in Fig. 2c) of thickness $RdD(t)$ binds to the surface of the fiber in an unstressed state. The reference length of the new stress-free layer equals the current fiber length $L_0\bar{\lambda}(t + dt)$, which is larger than the reference length of the core of the material $L_0\bar{\lambda}_g(t)$. Thus, releasing the macro-stretch $\bar{\lambda}(t + dt)$ returns the collagen fiber to a new reference length $\bar{\lambda}_g(t + dt)$, instead of $\bar{\lambda}_g(t)$. With this scenario in mind, a rate law describing the evolution of axial growth ratio $\bar{\lambda}_g(t)$ when $k_{dep}(t) - k_{deg}(t) > 0$ can be derived as follows. Upon unloading, the collagen fiber is overall stress-free, such that the resultant force on the fiber cross-section is zero, i.e., $\sigma_{core}\pi r(t)^2 + \sigma_{shell}2\pi r(t)R[k_{dep}(t) - k_{deg}(t)]dt = 0$. Note that in the growth configuration $\sigma_{core} = E\left[\frac{\bar{\lambda}_g(t+dt)}{\bar{\lambda}_g(t)} - 1\right]$ and $\sigma_{shell} = E\left[\frac{\bar{\lambda}_g(t+dt)}{\bar{\lambda}(t+dt)} - 1\right]$. Then linearizing the stretches at the current time as $\bar{\lambda}_g(t + dt) = \bar{\lambda}_g(t) + \dot{\bar{\lambda}}_g(t)dt$ and $\bar{\lambda}(t + dt) = \bar{\lambda}(t) + \dot{\bar{\lambda}}(t)dt$, combining these relations, and neglecting higher order dt terms give the following relation for the fiber growth stretch rate,

$$\frac{d\bar{\lambda}_g(t)}{dt} = 2\left[1 - \frac{\bar{\lambda}_g(t)}{\bar{\lambda}(t)}\right]\frac{\bar{\lambda}_g(t)}{D(t)}[k_{dep}(t) - k_{deg}(t)], \quad k_{dep}(t) - k_{deg}(t) > 0, \tag{7}$$

The fiber growth stretch rate scales with the net collagen deposition rate and decreases with increasing fiber radius, denoted by the radial growth ratio $D(t)$. A layer of unstressed material has a smaller effect on redistributing the axial stress inside a thicker fiber. We further assumed that the axial stress state in the collagen fiber homogenizes quickly after a layer of collagen is deposited on the fiber surface, such that the fiber exhibits a uniform reference (unstressed) length $\bar{\lambda}_g(t + \Delta t)$ in the cross section. As a result, subsequent degradation does not affect the fiber reference length.

In the case with a net degradation, $k_{dep}(t) - k_{deg}(t) \le 0$, no new collagen is deposited onto the fiber. Then the reference length $\bar{\lambda}_g(t + dt)$ remains $\bar{\lambda}_g(t)$, and the rate of the fiber growth stretch is zero,

$$\frac{d\bar{\lambda}_g(t)}{dt} = 0, \quad k_{dep}(t) - k_{deg}(t) < 0, \tag{8}$$

The degradation process by itself does not affect the collagen fiber length and thus the fiber grows in length only when the deposition rate exceeds the degradation rate. Solving Eqs. (6) and (7) together with initial condition $\bar{\lambda}_g(t = 0) = 1$ give the growth stretch $\bar{\lambda}_g(t)$ and diameter ratio $D(t)$ of individual collagen fibers. Equations (6)–(8) together form the fiber growth laws that we applied to develop a growth and remodeling model for a collagen network. Setting deposition rate equal to zero will reduce the fiber model, Eqs. (1)–(8), to the model developed by Tonge et al. for the enzymatic degradation of a collagen

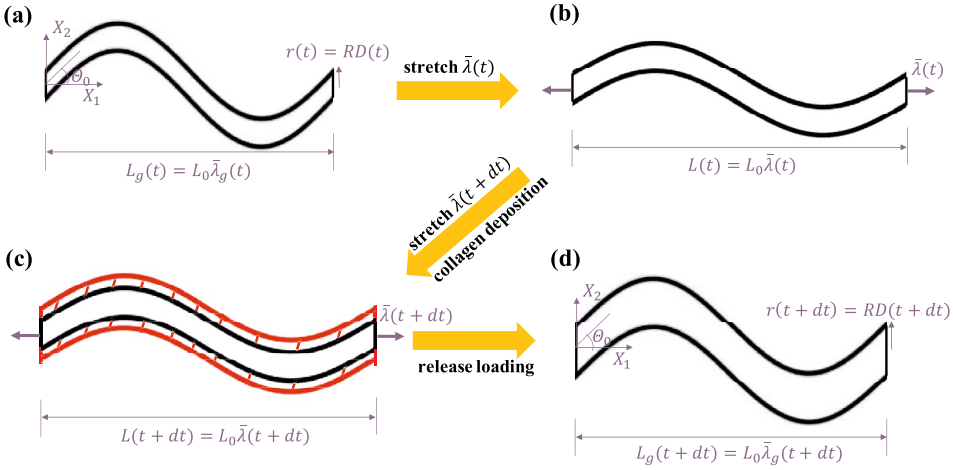

Fig. 2. Schematics of collagen deposition process and its effect on the axial growth ratio (a) The reference state (i.e., the growth state) of the collagen fiber at time t. (b) The deformed state of the fiber at time t. (c) Deformed state of fiber at time $t + dt$, with a new layer of collagen deposited on the fiber surface. (d) The new reference state of the fiber at time $t + dt$. Note that the crimp angle Θ_0 is assumed to be unaffected by the growth progress.

fiber (Tonge et al., 2015).

2.3. Growth and remodeling of a collagen fiber network

A distributed fiber modeling approach is applied to describe the anisotropic hyperelastic behavior of collagenous tissues. The tissue is conceptualized as a three-dimensional distribution of crimped collagen fibers embedded in an isotropic matrix composed of proteoglycans, elastin, and water. Let $\boldsymbol{\Omega}_0$ denotes the initial undeformed configuration of the collagenous tissue at time t_0 (before deposition, degradation, and deformation). We consider an infinitesimal representative volume element dV_0, i.e., an RVE, surrounding a material point $\boldsymbol{X} \in \boldsymbol{\Omega}_0$. The orientation of a collagen fiber in the RVE is described by a unit vector $\boldsymbol{a}_0(\vartheta, \phi) = \cos\vartheta\cos\phi\boldsymbol{e}_1 + \sin\vartheta\cos\phi\boldsymbol{e}_2 + \sin\phi\boldsymbol{e}_3$, where $\vartheta \in [0,2\pi]$ represents the circumferential angle and $\phi \in \left[-\frac{\pi}{2}, \frac{\pi}{2}\right]$ is the meridional angle, as illustrated in Fig. 1a. To describe the general 3D fiber distributions in collagenous tissues, we define an initial probability distribution function of the fiber orientation angles $\rho_0(\vartheta, \phi)$, such that $\int_0^{2\pi}\int_{-\pi/2}^{\pi/2} \rho_0(\vartheta, \phi)\sin\phi d\phi d\vartheta = 1$. In the following, the statistical average of a quantity $\langle\cdot\rangle$ is denoted as $\langle\cdot\rangle = \int_0^{2\pi}\int_{-\pi/2}^{\pi/2} (\cdot)\rho_0(\vartheta, \phi)\sin\phi d\phi d\vartheta$. The initial volume of fibers within the RVE can be evaluated as $dV_{f0} = \langle A_0 L_0 dN_f\rangle$, where $A_0(\vartheta, \phi)$ is the initial fiber cross-sectional area, $L_0(\vartheta, \phi)$ is the initial fiber contour length, and dN_f is the number of fibers in the RVE. Assuming that all fibers have the same initial cross-section area and length, the fiber volume can be written as $dV_{f0} = A_0 L_0 dN_f$. The RVE volume dV_0 in the initial configuration is the sum of the contribution from the crimped collagen fibers dV_{f0} and the contribution from the matrix dV_{m0}, namely, $dV_0 = dV_{f0} + dV_{m0}$. Therefore, we can define the initial fiber volume fraction as $\kappa_0 = dV_{f0}/dV_0$ and the initial matrix volume fraction as $1 - \kappa_0 = dV_{m0}/dV_0$.

At time $t > t_0$, the tissue under applied loading is subjected to elastic deformation, as well as growth induced by deposition and degradation. To describe the growth kinematics, an intermediate stress-free growth configuration $\boldsymbol{\Omega}_{\boldsymbol{g}}$ can be introduced. From $\boldsymbol{\Omega}_0$ to $\boldsymbol{\Omega}_{\boldsymbol{g}}$, collagen fibers grow through the process of deposition and degradation that changes both the fiber radius and length. In the growth configuration $\boldsymbol{\Omega}_{\boldsymbol{g}}$, the fiber volume in the RVE can be evaluated as $dV_{fg} = \langle A_g L_g dN_f\rangle = A_0 L_0 dN_f \langle D^2(\vartheta, \phi)\bar{\lambda}_g(\vartheta, \phi)\rangle$. By assuming for simplicity that the matrix does not grow, i.e., $dV_{mg} = dV_{m0}$, we can evaluate the volume of collagenous tissue in the growth configuration as $dV_g = dV_{mg} + dV_{fg} = dV_{m0} + dV_{f0}\langle D^2(\vartheta, \phi)\bar{\lambda}_g(\vartheta, \phi)\rangle$. The volumetric deformation of the tissue can thus be obtained as,

$$J^g = \frac{dV_g}{dV_0} = (1 - \kappa_0) + \kappa_0\langle D^2(\vartheta, \phi)\bar{\lambda}_g(\vartheta, \phi)\rangle, \tag{9}$$

The tissue-level deformation is characterized by the macroscopic deformation gradient tensor $\boldsymbol{F}$ which can be multiplicatively decomposed into a growth term and an elastic term, i.e., $\boldsymbol{F} = \boldsymbol{F^e F^g}$. $\boldsymbol{F^g}$ describes the tissue-level volume change due to fiber-level growth induced by deposition and degradation, and it is evident that J^g given in Eq. (9) equals $\det(\boldsymbol{F^g})$. $\boldsymbol{F^e}$ describes the elastic deformation of the tissue occurring from externally applied loads. To study the fiber-level deformation, the collagen fibers are assumed to deform affinely with the macroscopic deformation gradient $\boldsymbol{F}$. Thus, the macroscopic stretch of a collagen fiber with orientation ϑ and ϕ can be calculated as

$$\bar{\lambda}(\vartheta, \phi) = \sqrt{\boldsymbol{a}_0(\vartheta, \phi)\cdot\boldsymbol{C}\boldsymbol{a}_0(\vartheta, \phi)}, \tag{10}$$

where $\boldsymbol{C} = \boldsymbol{F^T F}$ is the right Cauchy-Green deformation tensor. We further assume that the fiber orientation vectors in the intermediate configuration $\boldsymbol{\Omega}_{\boldsymbol{g}}$ can be determined from an affine mapping by the growth deformation tensor $\boldsymbol{F^g}$, $\boldsymbol{a_g} = \frac{\boldsymbol{F^g a}_0}{\|\boldsymbol{F^g a}_0\|}$, such that the macroscopic fiber growth ratio is given by $\|\boldsymbol{F^g a}_0\| = \sqrt{\boldsymbol{a}_0\cdot\boldsymbol{C^g a}_0}$ (Nguyen et al., 2007), where $\boldsymbol{C^g} = (\boldsymbol{F^g})^T\boldsymbol{F^g}$ is the growth deformation tensor. By taking into account that the macroscopic growth stretch $\|\boldsymbol{F^g a}_0\|$ can be equated to the growth stretch ratio $\bar{\lambda}_g(t)$ of a fiber defined in Eqs. (7) and (8), the corresponding macroscopic elastic stretch of the fiber is thus given by

$$\bar{\lambda}_e(\vartheta, \phi) = \sqrt{\boldsymbol{a_g}\cdot\boldsymbol{C^e a_g}} = \frac{\sqrt{\boldsymbol{a}_0\cdot\boldsymbol{C a}_0}}{\sqrt{\boldsymbol{a}_0\cdot\boldsymbol{C^g a}_0}} = \frac{\bar{\lambda}(\vartheta, \phi)}{\bar{\lambda}_g(\vartheta, \phi)}, \tag{11}$$

It is important to choose the correct normalization volume for the strain energy density of tissues with changing volume and mass (Lubarda and Hoger, 2002). We define the strain energy density of the collagenous tissue on the intermediate growth configuration $\boldsymbol{\Omega}_{\boldsymbol{g}}$, since the strain energy density of the growth configuration represents the intrinsic material properties of the tissue. The strain energy density of the collagenous tissue consists of the contribution from the isotropic matrix and the contribution from the collagen fibers undergoing collagen deposition and enzymatic degradation. The isotropic and incompressible behavior of the matrix can be described by a Neo-Hookean hyperelastic potential $W_m = \frac{\mu}{2}(I_1 - 3)$, where μ is the matrix shear modulus and I_1 is the first invariant of $\boldsymbol{C}$. The strain energy density of collagen fibers can be determined by integrating the strain energy density of all fibers over all orientations weighted by the probability density distribution $\rho(\vartheta, \phi)$. Then, the strain energy density of the collagenous tissue per unit unstressed volume in the growth configuration $\boldsymbol{\Omega}_{\boldsymbol{g}}$ can be expressed as,

$$W = \frac{(1 - \kappa_0)}{J^g}W_m(\lambda_1^e, \lambda_2^e, \lambda_3^e) + \frac{\kappa_0}{J^g}\langle W_f(\bar{\lambda}_e(\vartheta, \phi))D^2(\vartheta, \phi)\bar{\lambda}_g(\vartheta, \phi)\rangle - p(J^e - 1), \tag{12}$$

where W_m is the strain energy density of the isotropic matrix, W_f is the strain energy density of the fibers defined by Eq. (4), p is the Lagrange multiplier enforcing the elastic incompressibility condition, $J^e = \frac{J}{J^g} = \lambda_1^e\lambda_2^e\lambda_3^e$ is the elastic volumetric deformation, $J = \det(\boldsymbol{F})$ is the total volumetric deformation. After defining the strain energy density W, the Cauchy stress can be derived as $\boldsymbol{\sigma} = \boldsymbol{F^e}\frac{\partial W}{\partial \boldsymbol{C^e}}(\boldsymbol{F^e})^T$,

$$\boldsymbol{\sigma} = \frac{(1 - \kappa_0)}{J^g}\mu\boldsymbol{b}^e + \frac{\kappa_0}{J^g}\langle\frac{1}{\bar{\lambda}_e}\frac{\partial W_f(\bar{\lambda}_e)}{\partial\bar{\lambda}_e}\boldsymbol{F^e a_g}\otimes\ \boldsymbol{F^e a_g}D^2\bar{\lambda}_g\rangle - p\boldsymbol{I}, \tag{13}$$

where $\boldsymbol{b^e} = \boldsymbol{F^e}(\boldsymbol{F^e})^T$ is the left Cauchy-Green deformation tensor and $\boldsymbol{I}$ is the identity tensor.

3. Results

3.1. Growth of collagen fibril under a constant applied force

We investigated the deformation and growth of a single collagen fiber subjected a constant applied force by solving Eqs. (1)–(3) for the fiber macroscopic stretch, diameter growth ratio and fiber growth stretch. Motivated by the experiments conducted by Flynn et al. (2010), the initial fiber diameter R were set to 275 nm and the constant force F was set to 46 nN. Material parameters such as Young's Modulus $E = 50$ MPa, initial slenderness ratio $\beta_0 = 4 \times 10^{-3}$, and initial crimp angle $\Theta_0 = 29°$ were determined previously by Tonge et al. (2015) for the equilibrium uniaxial tension response of bovine cornea strips (Zareian et al., 2010). We applied the intrinsic degradation rate $G_1 = 6.8 \times 10^{-4}\ \mathrm{s}^{-1}$ and the characteristic activation energy $G_2 = 700\ \mathrm{J/m^3}$ determined by Tonge et al. (2015) from enzymatic degradation experiments of collagen fibrils (Flynn et al., 2010). We further assumed $G_4 = 1000\ \mathrm{J/m^3}$ and $G_3 = 3 \times 10^{-4}\ \mathrm{s}^{-1}$ for the intrinsic activation energy and intrinsic rate of collagen deposition. These parameters are listed in Table 1 and were applied in all subsequent numerical examples unless stated otherwise.

To investigate how the interplay between deposition and degradation dictates the growth of a single crimped collagen fiber under a constant force, we simulated three cases with different intrinsic deposition rate of G_3: $1 \times 10^{-4}\ \mathrm{s}^{-1}$ for slow deposition (Fig. 3), $3 \times 10^{-4}\ \mathrm{s}^{-1}$ for the baseline case (Fig. 4), and $8 \times 10^{-4}\ \mathrm{s}^{-1}$ for fast deposition

Table 1
Material parameters for collagen fibers and tissues.

Elastica Parameters	E	Fiber Young's Modulus	50 MPa
	β_0	Fiber slenderness ratio	4×10^{-3}
	Θ_0	Initial fiber crimp angle	29°
Degradation and Deposition Parameters	G_1	Intrinsic degradation rate	6.8×10^{-4} s^{-1}
	G_2	Characteristic degradation energy	700 J/m^2
	G_3	Intrinsic deposition rate	3×10^{-4} s^{-1}
	G_4	Characteristic deposition energy	1000 J/m^2

(Fig. 5). Fig. 3a shows the evolution of deposition (red dashed line) and degradation (blue solid line) rates over time for the case $G_3 = 1 \times 10^{-4}$ s^{-1}. As indicated by Eq. (5), both deposition and degradation rates are enhanced and reduced respectively by the axial strain energy density W_{axial} of the collagen fiber. At time $t = 0$, the stretch induced by the applied force led to an initial degradation rate of $\beta(0) = 4.05 \times 10^{-4}$ and a lower initial deposition rate of $\alpha(0) = 1.44 \times 10^{-4}$ (Fig. 3a). The resulting net degradation of the fiber radius (Fig. 3b) induced a reduction in the slenderness ratio β and caused the fiber to gradually straighten and creep under the constant force, giving rise to further reduction and enhancement of the degradation and deposition rates. Equilibrium was attained when the increasing deposition rate reached the decreasing degradation rate. Moreover, axial growth was inhibited, i.e., $\bar{\lambda}_g(t) = 1$, because collagen degradation dominated deposition (Fig. 3c). Thus, the elastic stretch $\bar{\lambda}_e(t) = \bar{\lambda}(t)$ for all time (Fig. 3d). At $t = 0$, the $\bar{\lambda}_e(0)$ and $\bar{\lambda}(0)$ represent the instantaneous elastic stretch and instant total stretch in response to the application of the force F.

For the baseline case with larger intrinsic deposition rate $G_3 = 3 \times 10^{-4}$ s^{-1}, the initial deposition rate after the application of F were $\alpha(0) = 4.31 \times 10^{-4}$. The initial degradation rate $\beta(0) = 4.05 \times 10^{-4}$ was smaller, which yielded a net deposition (Fig. 4a). The net deposition increased the fiber radius (Fig. 4b), which reduced the strain energy density W_{axial}. Material equilibrium was reached when the deposition rate equaled the degradation rate, as shown in Fig. 4a. Growth increased the fiber radius by 1.8% (Fig. 4b) and the fiber length by 0.18% (Fig. 4c). In contrast to the first case, the elastic fiber stretch $\bar{\lambda}_e(t)$ decreased while the total stretch $\bar{\lambda}(t) = \bar{\lambda}_e(t)\bar{\lambda}_g(t)$ increased with time before reaching equilibrium.

Finally, we simulated the growth of a fiber with a high intrinsic deposition rate $G_3 = 8 \times 10^{-4}$ s^{-1}. The growth of the fiber did not attain a material equilibrium (Fig. 5b-c) because the deposition rate was so large that it could not be balanced by the degradation rate (Fig. 5a). The elastic fiber stretch $\bar{\lambda}_e(t)$ continued to decrease towards $\bar{\lambda}_e = 1$ and the total fiber stretch $\bar{\lambda}(t)$ also showed a drastic drop after an initial increase (Fig. 5d), which were both attributed to the continuous thickening of collagen fiber. The unbounded growth in the fiber radius shown in Fig. 5b is likely not physical. The assumption that a constant collagen deposition rate leading to a constant rate of growth of the fiber radius would break down for large fibers. The fiber growth rate also could be inhibited by the surface energy of the fiber, which would increase with increasing surface area. Investigating the influence of surface energy on the growth of collagen fibers is beyond the scope of this paper and requires future exploration.

3.2. Growth of collagen fiber under cyclic loading

We next investigated the growth of a collagen fiber subjected to cyclic loading, which is the physiological loading conditions of most tissues. Experiments have shown that cyclic loading can play an

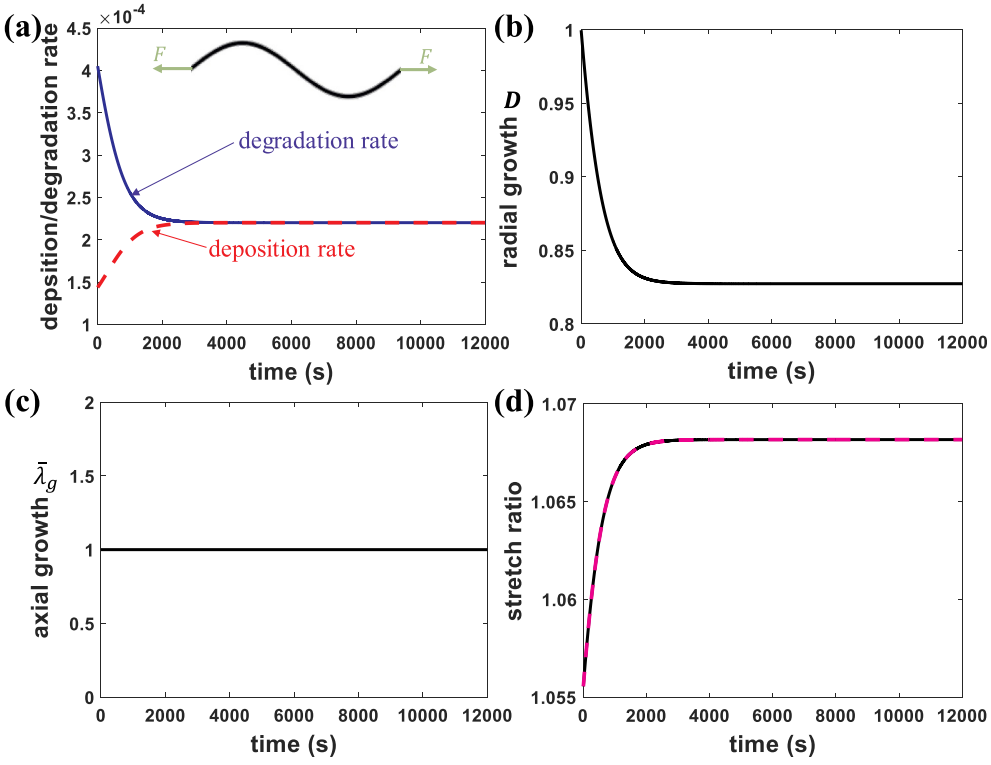

Fig. 3. The effect of collagen deposition on the growth of a single collagen fiber under a constant force loading. The intrinsic deposition rate (deposition rate with zero stress) $G_3 = 1 \times 10^{-4}$ s^{-1} to denote a relatively slow deposition. (a) Once the force $F = 46$ nN is applied, the fiber deforms and the initial deposition is slower than the degradation. The applied force gradually reduces the degradation rate while increases the deposition rate. The equilibrium state of growth is reached when the degradation rate is reduced to the level of the deposition rate. (b) The fiber radius keeps decreasing over time before attaining equilibrium. (c) The axial growth ratio $\bar{\lambda}_g(t)$ remains to be 1 since the prevailing degradation inhibits the axial growth. (d) The fiber creeps under the constant force, with the total and elastic stretch ratios both increasing until equilibrium is reached.

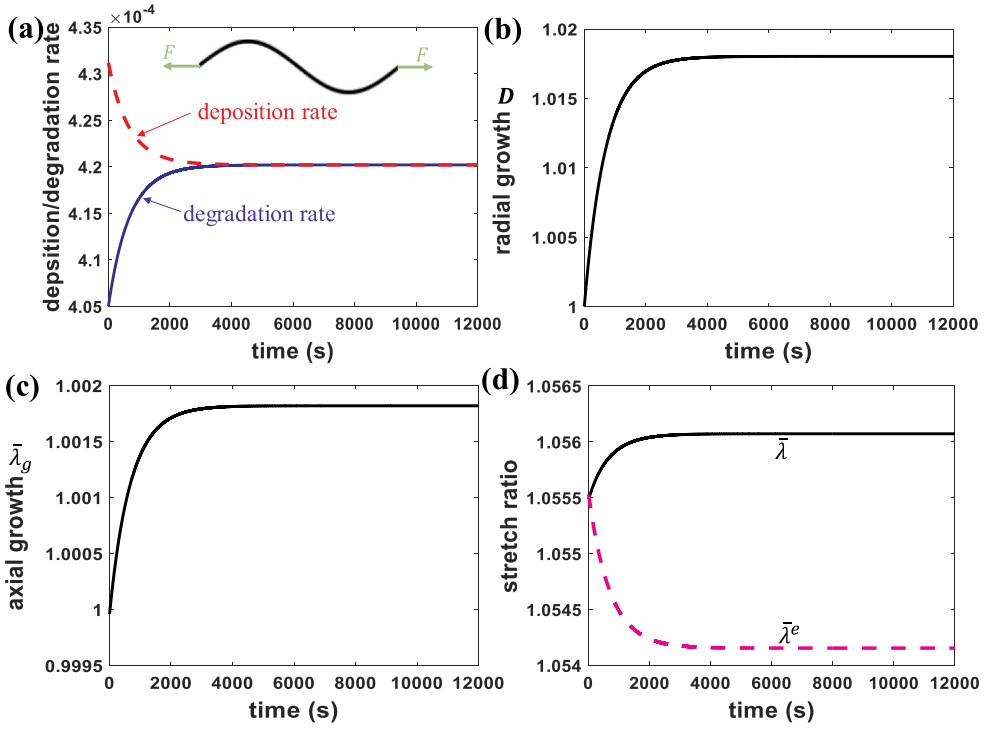

Fig. 4. The effect of collagen deposition rate on the growth of single collagen fiber. The intrinsic deposition rate G_3 is taken to be $3 \times 10^{-4}\ s^{-1}$. (a) The deposition prevails over the degradation, resulting in a net deposition before the equilibrium state is attained. As a result, (b) the fiber radius increases over time, and (c) the fiber length grows axially. (d) The elastic fiber stretch decreases with time under a constant force because fiber radius increases.

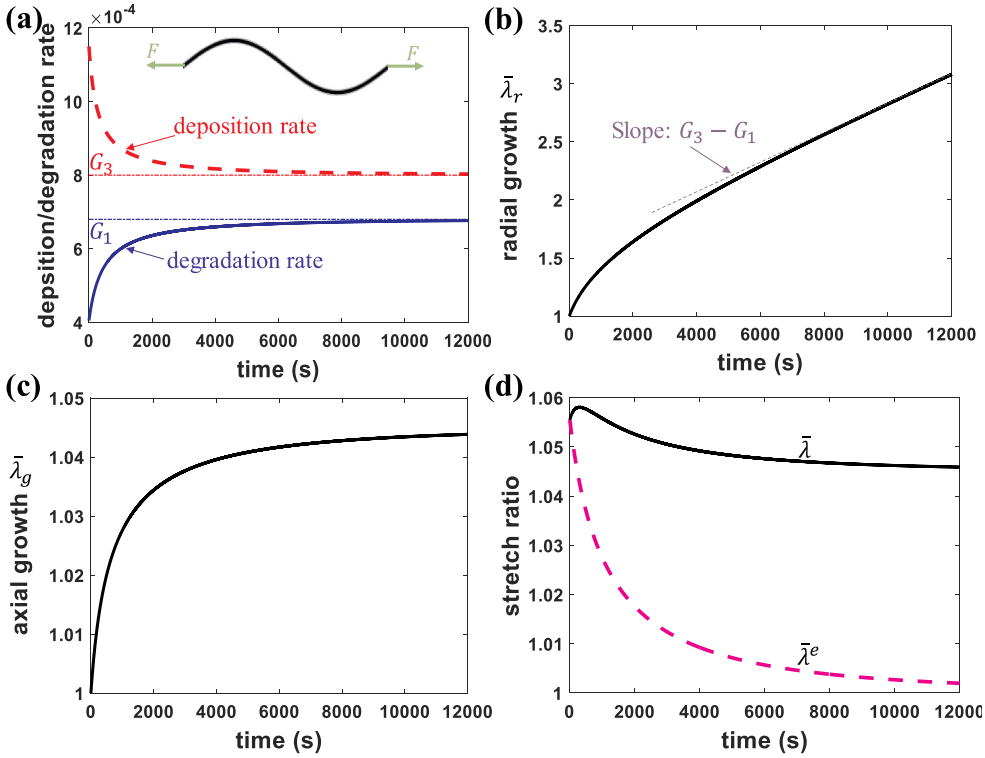

Fig. 5. Growth of a single collagen fiber subjected to fast deposition with intrinsic deposition rate of $G_3 = 8 \times 10^{-4}\ s^{-1}$. (a) The deposition dominates over the degradation and the growth did not attain material equilibrium, since the intrinsic deposition rate G_3 is higher than the intrinsic degradation rate G_1. (b) The fiber radius increases over time. The slope of the curve decreases gradually and eventually reduces to $G_3 - G_1$. (c) The fiber also grows unboundedly in the axial direction. (d) Because of the increasing cross-section area, the elastic stretch ratio decreases and the total stretch ratio also decreases after an initial increase.

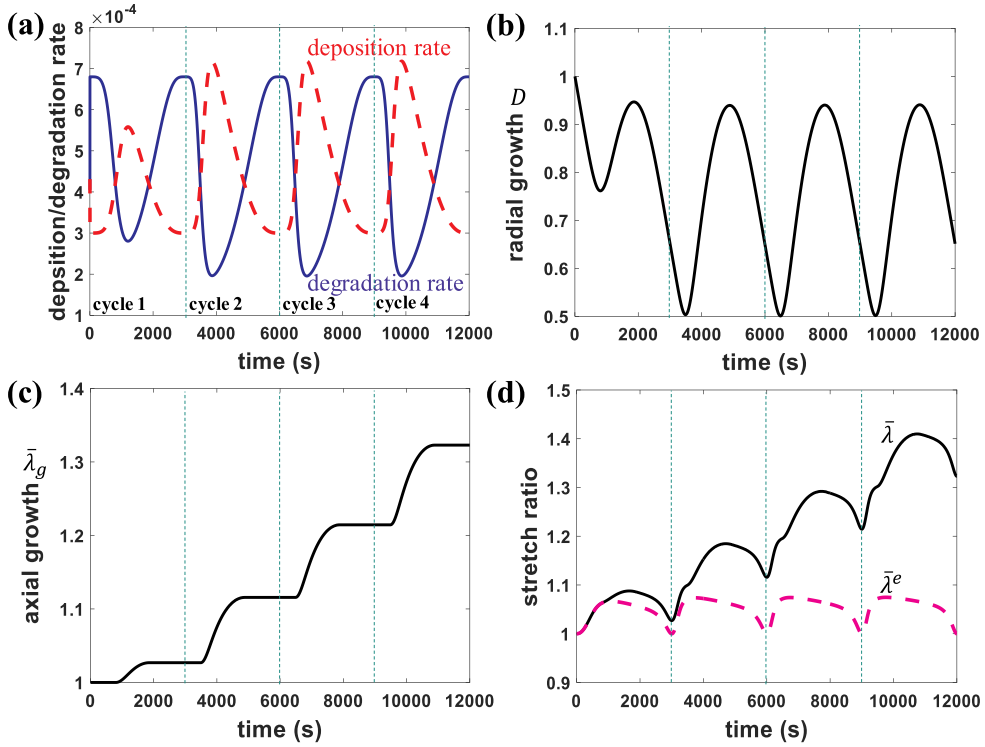

Fig. 6. Growth of a collagen fibril subjected to cyclic force that with mean 23 nN and amplitude 46 nN. (a) The deposition and degradation rates and (b) the radial growth achieved dynamic equilibrium, where D oscillates about a mean. (c) The axial growth stretch and total stretch accumulated with each cycle, exhibiting a ratcheting behavior, and did not achieve equilibrium.

important role in tissue development, growth and remodeling and maintenance (Mubyana and Corr, 2018; Susilo et al., 2016; Wong et al., 2003). Smooth-muscle cells are observed to exhibit an increase in production of type-I and type-II collagen molecules when subjected to cyclic stretching (Miller et al., 2005). In this section, we investigated the growth of a collagen fiber, with initial radius $R = 275$ nm, subjected to a cyclic force, $F = F_0\left(1 - \cos\frac{2\pi}{T}t\right)$, where $T = 3000$ s denotes the period and $F_0 = 23$ nN is the mean amplitude of the force.

The cyclic loading caused the mechanics-inhibited degradation and mechanics-stimulated deposition rates to cycle out of phase with each other by 180° (Fig. 6a). The alternating net deposition and net degradation conditions led to the cyclic variation of fiber radius ratio that reached steady-stated after the second cycle (Fig. 6b). In contrast, the axial growth stretch increased with each cycle because the growth law is biased to allow axial growth only when the deposition rate is greater than the degradation rate (Fig. 6c). The elastic fiber stretch $\bar{\lambda}^e$ varied with the applied cyclic force, which caused the total fiber stretch $\bar{\lambda}$ to increase with each cycle (Fig. 6d). At the beginning of the cycle, the total stretch increased because of elastic loading until the deposition rate exceeded the degradation rate. Then, the increase in the fiber stretch was caused mainly by axial growth. The fiber stretch decreased at the end of the loading cycle because of elastic unloading. The results suggest that cyclic loading is essential for enabling the continual axial growth of the collagen fiber, while a growth under a static load force results in the development of a material equilibrium. While we used a low frequency corresponding to a time period of 3000s, continuous fiber growth would be observed at any loading frequency.

3.3. Effect of collagen deposition and degradation on the tissue homeostasis

In this section, we investigated the growth and homeostasis of an thin spherical collagenous membrane subjected to a time-dependent inner pressure $P(t)$, under concurrent collagen deposition and degradation (Fig. 6a). To approximate the dimensions of the human sclera and the intraocular pressure, the initial radius and wall thickness of the membrane are taken to be $R_m = 12.5$ mm and $H_m = 1$ mm, respectively. We assumed that all the collagen fibers are arranged isotropically in the plane of tissue (i.e., $\phi = 0$ in Fig. 1a).

The stress response for the tissue given in Eq. (13) is composed of an isotropic part attributed to the compliant matrix of water, cells proteoglycans and other non-fibril forming proteins and an anisotropic part attributed to the fibers. The parameters in Table 1 were used to describe the material properties and degradation/deposition kinetics of the collagen fibers. We assumed that the matrix was very compliant compared to the fiber phase, such that $(1 - \kappa_0)\mu \ll \kappa_0 E$. Then neglecting the matrix response and setting $\kappa_0 = 1$ for simplicity gives the following for the tissue stress response,

$$\boldsymbol{\sigma} = \frac{1}{J^g}\langle\frac{1}{\bar{\lambda}_e}\frac{\partial W_f(\bar{\lambda}_e)}{\partial\bar{\lambda}_e}\boldsymbol{F}^e\boldsymbol{a}_g \otimes \boldsymbol{F}^e\boldsymbol{a}_g D^2\bar{\lambda}_g\rangle - p\boldsymbol{I} \tag{14}$$

When subjected to an inner pressure, the thin spherical tissue is under equibiaxial tension, with the following deformation gradient,

$$\boldsymbol{F} = \lambda_{11}\boldsymbol{e}_1 \otimes \boldsymbol{e}_1 + \lambda_{22}\boldsymbol{e}_2 \otimes \boldsymbol{e}_2 + \lambda_{33}\boldsymbol{e}_3 \otimes \boldsymbol{e}_3 \tag{15}$$

$$\boldsymbol{F} = \lambda^e_{11}\lambda^g_{11}\boldsymbol{e}_1 \otimes \boldsymbol{e}_1 + \lambda^e_{22}\lambda^g_{22}\boldsymbol{e}_2 \otimes \boldsymbol{e}_2 + \lambda^e_{33}\lambda^g_{33}\boldsymbol{e}_3 \otimes \boldsymbol{e}_3 \tag{16}$$

Note that $\boldsymbol{e}_1$ and $\boldsymbol{e}_2$ are located in the tissue plane and $\lambda_{11} = \lambda_{22} = \lambda$ denotes the total hoop stretch of the thin spherical tissue with an isotropic in-plane fiber distribution. The tissue-level volumetric ratio $J^g = \lambda_{11}\lambda_{22}\lambda_{33} = \lambda^g_{11}\lambda^g_{22}\lambda^g_{33}$ is connected to the fiber-level growth by Eq. (9). The term p in Eq. (14) can be determined by considering the plane stress condition, i.e., $\sigma_{33} = 0$. Taking these into account, the in-plane stresses of the thin spherical collagenous tissue are given by,

$$\sigma_{11} = \sigma_{22} = \frac{1}{J^g}\langle\bar{\lambda}_e\frac{\partial W_f(\bar{\lambda}_e)}{\partial\bar{\lambda}_e}\frac{\lambda^2\cos^2\cos^2\vartheta}{\bar{\lambda}^2}D^2\bar{\lambda}_g\rangle - J^g\langle\bar{\lambda}_e\frac{\partial W_f(\bar{\lambda}_e)}{\partial\bar{\lambda}_e}\frac{\sin^2\phi}{\lambda^4\bar{\lambda}^2}D^2\bar{\lambda}_g\rangle \tag{17}$$

Detailed derivations of Eq. (17) are provided in Section B of the supporting information.

The tissue hoop stresses in a thin spherical membrane subjected to an inner pressure $P(t)$ is given by $\sigma_{11} = \sigma_{22} = \frac{Pr_m}{2h_m} = \frac{PR_m\lambda^3}{2H_mJ^g}$, where r_m and h_m are the spherical tissue radius and wall thickness of the membrane tissue in the current configuration. The stretch $\lambda_{11} = \lambda_{22} = \lambda$ can be determined by solving the nonlinear relation,

$$\frac{PR_m\lambda^3}{2H_mJ^g} = \frac{1}{J^g}\langle\bar{\lambda}_e\frac{\partial W_f(\bar{\lambda}_e)}{\partial\bar{\lambda}_e}\frac{\lambda^2\cos^2\cos^2\vartheta}{\bar{\lambda}^2}D^2\bar{\lambda}_g\rangle - J^g\langle\bar{\lambda}_e\frac{\partial W_f(\bar{\lambda}_e)}{\partial\bar{\lambda}_e}\frac{\sin^2\phi}{\lambda^4\bar{\lambda}^2}D^2\bar{\lambda}_g\rangle \tag{18}$$

where the elastic fiber stretch was defined as, $\bar{\lambda}_e = \bar{\lambda}/\bar{\lambda}_g$. The fiber stretch $\bar{\lambda}$ can be computed from the total stretch using Eq. (10). The fiber growth stretch $\bar{\lambda}_g$ equals to $\lambda_{11}^g = \lambda_{22}^g$ for equibiaxial loading. Solving the above relation requires solving for the internal variables for the normalized fiber force α using Eqs. (1)–(3), the fiber radius growth ratio D using Eq. (6) and the fiber growth stretch $\bar{\lambda}_g$ using Eqs. (7) and (8). More numerical details about solving tissue stretches can be found in Section C and D of the supporting information.

To investigate the development of homeostatic stress state, the spherical membrane was subjected to a constant pressure $P(t) = 2$ kPa for 5000s to allow the deposition and degradation process to develop an equilibrium state. After 5000 s, a step increase in the pressure of $\Delta P = 0.25$ kPa was applied to raise the pressure to 2.25 kPa. After 10000 s, the pressure was reduced to 1.9 kPa by a step decrease of $\Delta P = -0.35$ kPa. The deposition/degradation kinetics and the tissue stresses and strains for the loading history are plotted in Figs. 7–8. For $t < 5000$ s, the degradation rate of collagen fibers in the tissue plane was higher than the deposition rate. The net degradation reduced the fiber cross-section area, which decreased the fiber volume fraction and stiffness. This caused the tissue stretch and stress to increase until they attained equilibrium where the mechanically inhibited degradation rate balanced the mechanically stimulated deposition rate. The sudden increase in pressure at $t = 5000$ s, produced a jump in the deposition rate and a drop in the degradation rate, resulting in a net deposition. The resulting thickening of the tissue caused the hoop stress and elastic strain to decrease back to an equilibrium state (Fig. 7c–d). The hoop stress recovered the initial equilibrium response (see the inset of Fig. 7c), while the equilibrium value for the hoop strain was smaller than before the pressure perturbation (inset of Fig. 7d). The step pressure decrease to $P = 1.9$ kPa at $t = 10000$ s, caused an instantaneous drop in the hoop stretch and stress. It also caused collagen degradation to occur initially faster than deposition, which caused the hoop stress and strain to gradually increase towards equilibrium. As highlighted in the inset of Fig. 7c, the equilibrium hoop stress was restored to the initial equilibrium value. In contrast, the equilibrium elastic stretch at $P = 1.9$ kPa was larger than the value at $P = 2$ kPa and $P = 2.25$ kPa. Thus, the model was able to produce the development of stress homeostasis, where the stress recovered the initial equilibrium value, after an increase and decrease in pressure without prescribing a target stress or target fiber stretch as a model parameter. The stress recovered the homeostatic value in about 25 min, which was similar to the stress recovery time observed by Ezra et al. (2010) but significantly faster than measured by Brown et al. (Brown et al. (1998). Cyron et al. (2016) fit a homogenized constrained mixture for the exponential stress recovery to a target stress and obtained a characteristic recovery time of 1 h for the fibroblast seeded gel experiment of Ezra et al. (2010) and 11 h for Brown et al. (Brown et al. (1998). The difference in the characteristic

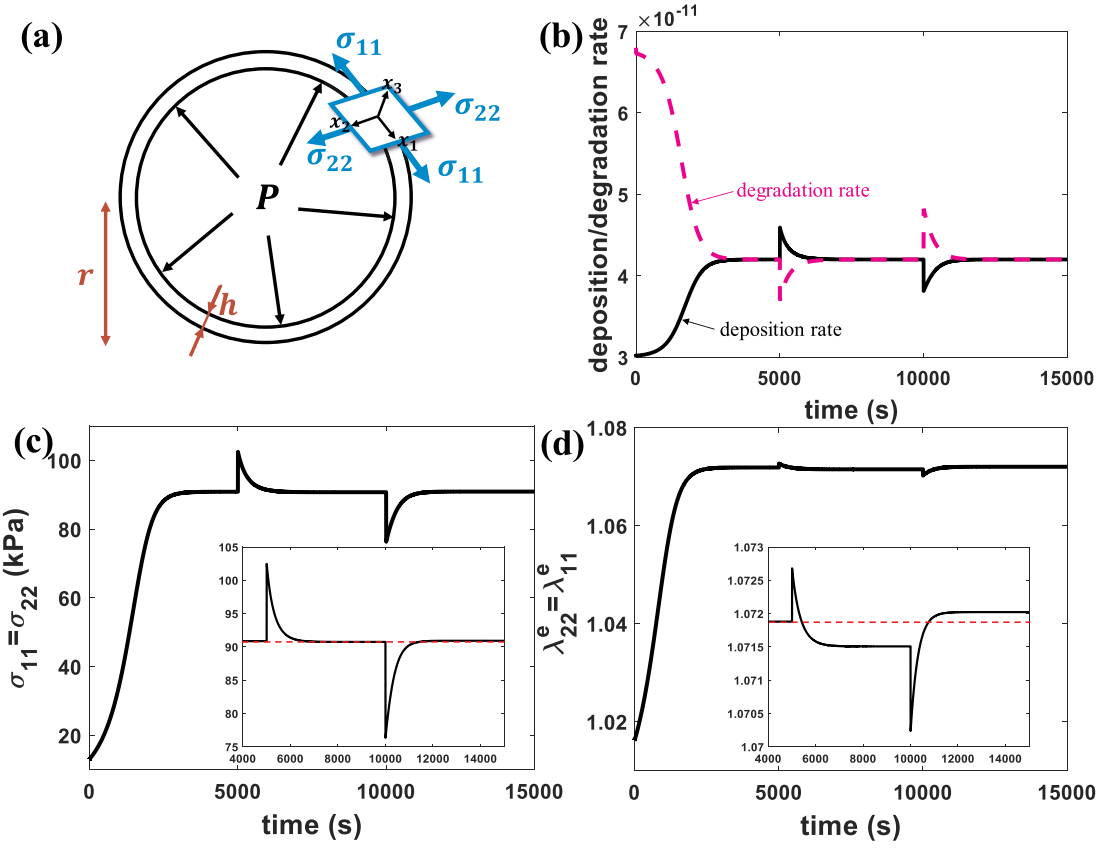

Fig. 7. Effect of pressure perturbation on the mechanical response of the tissue. (a) Schematics of a thin spherical collagenous tissue which is an approximation of the human sclera. The inner pressure P is held at 2 kPa for 5000 s, then raised to 2.25 kPa at $t = 5000$ s, followed by a reduction to 1.9 kPa at $t = 10000$ s. (b) Under the pressure perturbation, degradation and deposition dominate alternatingly. Equilibrium states are reached when collagenous deposition balances the enzymatic degradation. (c) Stress homeostasis is attained (see the inset, the red dashed line is for eye guidance). (d) Strain homeostasis is not reached as evident by the inset.

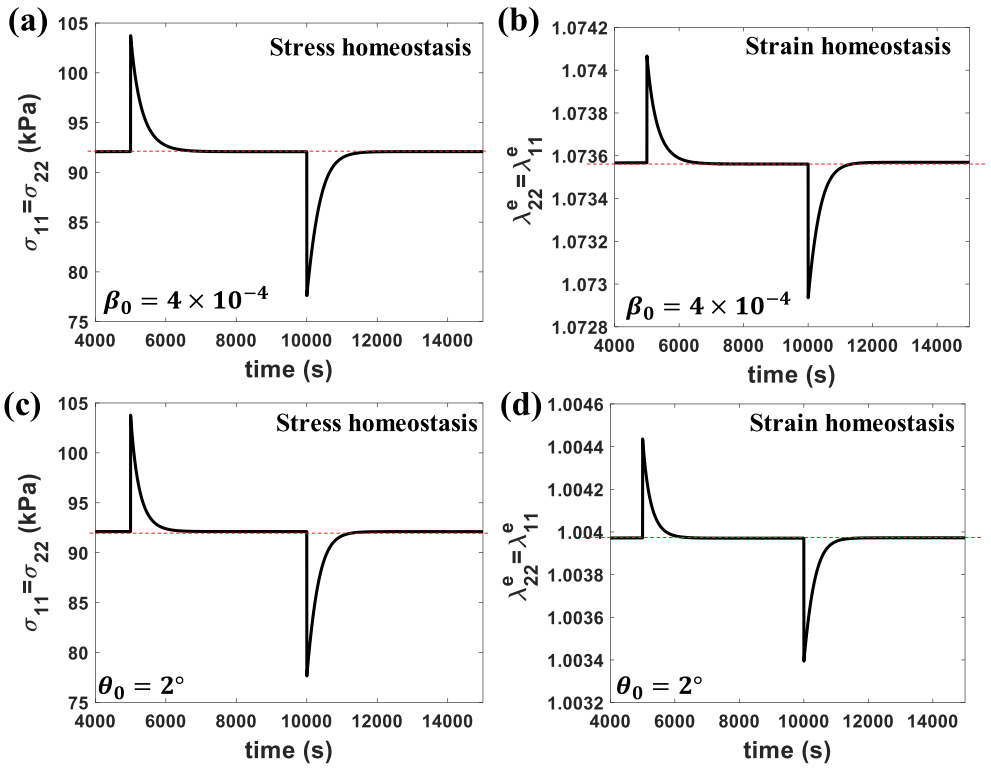

Fig. 8. Effect of slenderness ratio and crimp angle on the stress and strain homeostasis. Stress and strain homeostasis can be attained simultaneously for a fiber with a smaller slenderness ratio of $\beta_0 = 4 \times 10^{-4}$ (a, b) or a smaller crimp angle $\theta_0 = 2°$ (c, d).

recovery time was hypothesized to be caused by the difference in the cell density in the collagen gels. The recovery time in the model are affected by the parameters for the intrinsic degradation and deposition rates and the activation energies for mechanical inhibition of enzymatic degradation and mechanical stimulation of deposition. For instance, the recovery time is about 7 min for degradation inhibition energy $G_2 = 70$ J/m^3, 25 min for $G_2 = 700$ J/m^3, and 58mins for $G_2 = 70000$ J/m^3, indicating that larger G_2 leads to a longer recovery time. The recovery time can be increased also by decreasing the deposition stimulation energy G_4. The effects of cell density in the tensional homeostasis experiments can be incorporated through the parameters for the intrinsic degradation rate and activation energy for mechanical stimulation.

The numerical example did not achieve strain homeostasis. A different equilibrium elastic strain was obtained after each pressure perturbation (Fig. 7d), while a homeostatic stress was recovered (Fig. 7c). A possible explanation for the phenomenon is that the stress and strain response of the tissue depend on the fiber radius growth ratio D and axial growth stretch $\bar{\lambda}_g$ through the bending strain energy, $W_{bending}$. Both D and $\bar{\lambda}_g$ changed over time such that the strain could not recover its initial equilibrium value when the stress attained homeostasis. However, if we considered a more slender fiber with an order of magnitude smaller slenderness ratio of $\beta_0 = 4 \times 10^{-4}$, the influence of D and $\bar{\lambda}_g$ through the bending energy term $W_{bending}$ became negligible. Therefore, strain and stress homeostasis could be attained simultaneously, as evident in Fig. 8a and b. Likewise, a fiber with a much smaller crimp angle of $\theta_0 = 2°$ can also attain both stress and strain homeostasis in response to the same pressure perturbation (Fig. 8c and d).

For the thin spherical shell examined here with an isotropic, predominantly planar distribution of collagen fibers, the tissue growth stretch was the same as the growth stretch of the fibers (Fig. 9). The current tissue radius and thickness of the spherical tissue membrane can be given by $r_m = R_m \lambda^g_{11}$ (Fig. 9a) and $h_m = H_m \lambda^g_{33} = H_m \frac{J^g_s}{\lambda^2_{11}}$ (Fig. 9b). The change in the thickness depends on both the fiber axial growth stretch and the fiber radius growth ratio D. The tissue radius grew by 0.9% in response to an increase in pressure, but did not shrink after the decrease in pressure because of the bias in the growth law for collagen fibers. In contrast, the thickness increased after the pressure increase and decreased after the pressure decrease because fiber radius growth ratio D can increase and decrease under net deposition and net degradation conditions.

4. Conclusion

We developed a micromechanical model to investigate the growth and remodeling of collagenous tissues under concurrent collagen deposition and degradation. The collagen tissue is considered as a 3D distribution of crimped cylindrical collagen fibers. We hypothesize that the radius of the collagen fibers can shrink when there is a net degradation rate and that the radius and length of the collagen fiber can grow when there is a net deposition rate. We further assumed that collagen degradation is inhibited by the axial strain energy of the collagen fibers, and used the parameters determined by Tonge et al. (2015) from the experiments of Flynn et al. (2010) for the force inhibition of the degradation of collagen fibrils and Zareian et al. (2010) for a cornea strip. We first applied the fiber-level growth model to study the evolution of radius and length of a crimped collagen fiber subjected to either a constant force or a cyclic force, under simultaneous collagen deposition and degradation. The fiber-level model was incorporated into a tissue-level micro-mechanical model to study the development of stress and strain homeostasis of thin spherical collagenous tissue in response to an increase and decrease in pressure. The major findings of the present study are summarized below.

- The axial growth of collagen fiber depends on the competition between deposition and degradation. A collagen fiber subjected to a static force reaches an equilibrium state, when the deposition balances the degradation. In the equilibrium state, the fiber radius and

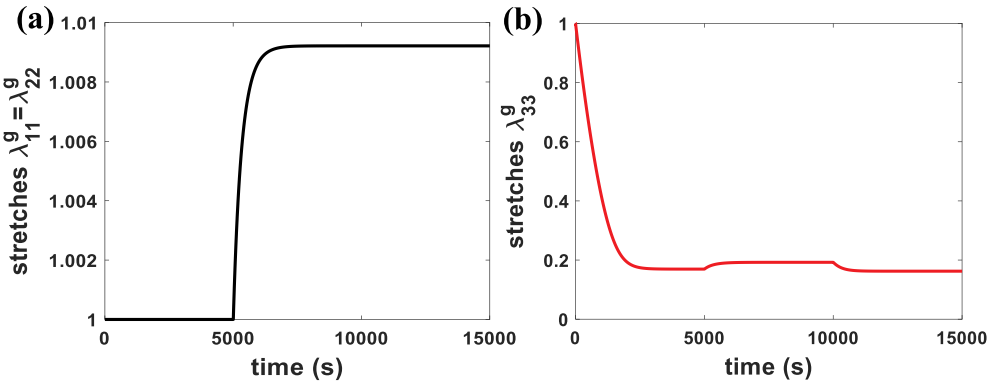

Fig. 9. Effect of pressure perturbation on the tissue dimensions. (a) The tissue radius in the growth configuration (b) The tissue thickness in the growth configuration.

length both attain a steady-state value.

- The length of collagen fibers subjected to cyclic force loading grows with each load cycle, which indicates that a cyclic force can effectively drive continual axial growth of fibers.
- It is predicted by our model that the deposition and degradation may work synergistically to maintain the tissue homeostasis. The idealized thin spherical tissue studied in this work can attain an equilibrium of stress and strain level after perturbations in pressure. However, only the stress recovers the initial equilibrium value before perturbation. This indicated the model can produce stress homeostasis without prescribing a homeostatic target as a parameter. Strain homeostasis was achieved when the slenderness ratio or the crimp angle was decreased significantly, which shows a possible effect of fiber morphology on the development of homeostasis

The present model can capture many important phenomena of growth and remodeling observed in soft collagenous tissues using only 2 mechanisms, the mechanical inhibition of enzymatic degradation of collagen and mechanical stimulation of collagen deposition. The latter describes an important mechanosensitive function of fibroblasts. However, the model does not currently include the effect of cellular traction of the extracellular matrix, which may be important in modeling matrix contraction and the reorientation of fibers. The characteristic time for the growth and remodeling behavior to reach equilibrium is determined directly by the rates of degradation and deposition and indirectly by the fiber crimp morphology and mechanical properties through the effect of mechanical inhibition of degradation and mechanical stimulation of deposition. Growth and remodeling may involve additional processes with different characteristic times, such that characteristic time of stress recovery may be different from the kinetics of degradation and deposition. The model includes assumptions of molecular deposition that currently lack experimental validation. For example, we assumed that collagen molecules are deposited onto the surface of a collagen fiber in an unstressed state. A nonzero deposition stretch would not qualitatively change the model findings as long as it is below the fiber stretch. Another important assumption of the model is that collagen fibers can grow in length under a net deposition rate, but cannot shrink in length under a net degradation rate. This allowed for continued axial growth of the fiber under cyclic loading but prevents the fiber from shrinking axially under load. In the membrane simulation, the assumption allowed the radius of the spherical tissue membrane in the numerical example to grow in respond to an increase in pressure, but it cannot shrink in response to a decrease in pressure. The model predicted that the thickness of the membrane would increase under an increase in pressure. However, we measured that the sclera of mouse eyes subjected to long-term IOP elevation can increase or decrease depending on the mouse type and region of the sclera (Nguyen et al., 2013). The collagen network model also exhibits a number of limitations. The collagen fibers are assumed to deform affinely with the macroscopic deformation of collagenous tissue and the mechanical interactions between fibers are not taken into account. Chang and Buehler (2014) showed that a collagen molecule behaves like a worm-like chain, with little load bearing capacity in compression. However, we assumed for simplicity a linear elastic axial stress-stretch response for the collagen monomer and fiber. Damage arising from mechanical loadings (e.g., Chen et al., 2018) is not considered either. Moreover, all collagen fibers are assumed to have the same crimp angle as well as the same initial length and radius, rather than a distribution of crimp angles, lengths and radii. Some of these limitations can be addressed by incorporating the evolution equations for the radius growth ratio and axial growth stretch of the fiber into a discrete network model. Despite these limitations, this relatively simple micromechanical growth and remodeling model shows how concurrent collagen degradation and deposition can produce stress homeostasis without a prescribed target stress and how the mechanical properties of the collagen fiber can affect the development of the homeostatic state.

Acknowledgements

Thao D. Nguyen acknowledges support from the National Science Foundation CAREER Award No. 1253453. Both Zheng Jia and Thao D. Nguyen acknowledge the Johns Hopkins University 2016 Catalyst Award. Zheng Jia also acknowledges the financial support from the One-hundred Talents Program of Zhejiang University and the Fundamental Research Funds for the Central Universities in China.

Appendix A. Supplementary data

Supplementary data to this article can be found online at https://doi.org/10.1016/j.jmbbm.2019.06.004.

References

Adhikari, A.S., Chai, J., Dunn, A.R., 2011. Mechanical load induces a 100-fold increase in the rate of collagen proteolysis by MMP-1. J. Am. Chem. Soc. 133, 1686–1689.
Alperin, N., Bagci, A.M., 2018. Spaceflight-induced visual impairment and globe deformations in astronauts are linked to orbital cerebrospinal fluid volume increase. Acta Neurochir. Suppl. 126, 215–219.
Baek, S., Rajagopal, K.R., Humphrey, J.D., 2006. A theoretical model of enlarging intracranial fusiform aneurysms. J. Biomech. Eng. Trans. ASME 128, 142–149.
Bhole, A.P., Flynn, B.P., Liles, M., Saeidi, N., Dimarzio, C.A., Ruberti, J.W., 2009. Mechanical strain enhances survivability of collagen micronetworks in the presence of collagenase: implications for load-bearing matrix growth and stability. Phil. Trans. Math. Phys. Eng. Sci. 367, 3339–3362.
Boote, C., Hayes, S., Jones, S., Quantock, A.J., Hocking, P.M., Inglehearn, C.F., Ali, M., Meek, K.M., 2008. Collagen organization in the chicken cornea and structural alterations in the retinopathy, globe enlarged (rge) phenotype - an X-ray diffraction study. J. Struct. Biol. 161, 1–8.
Brown, I.A., 1972. Scanning electron-microscopy of human dermal fibrous tissue. J. Anat. 113, 159–168.
Brown, R.A., Prajapati, R., McGrouther, D.A., Yannas, I.V., Eastwood, M., 1998. Tensional homeostasis in dermal fibroblasts: mechanical responses to mechanical loading in

three-dimensional substrates. J. Cell. Physiol. 175, 323–332.
Chang, S.-W., Buehler, M.J., 2014. Molecular biomechanics of collagen molecules. Mater. Today 17, 70–76.
Chen, M.L., Ruberti, J.W., Nguyen, T.D., 2018. Increased stiffness of collagen fibrils following cyclic tensile loading. J. Mech. Behav. Biomed. Mater. 82, 345–354.
Chiquet, M., Reneda, A.S., Huber, F., Fluck, M., 2003. How do fibroblasts translate mechanical signals into changes in extracellular matrix production? Matrix Biol. 22, 73–80.
Comninou, M., Yannas, I.V., 1976. Dependence of stress-strain nonlinearity of connective tissues on geometry of collagen-fibers. J. Biomech. 9, 427–433.
Cyron, C.J., Aydin, R.C., Humphrey, J.D., 2016. A homogenized constrained mixture (and mechanical analog) model for growth and remodeling of soft tissue. Biomechanics Model. Mechanobiol. 15, 1389–1403.
Cyron, C.J., Humphrey, J.D., 2014. Vascular homeostasis and the concept of mechanobiological stability. Int. J. Eng. Sci. 85, 203–223.
Cyron, C.J., Humphrey, J.D., 2017. Growth and remodeling of load-bearing biological soft tissues. Meccanica 52, 645–664.
Demirkoparan, H., Pence, T.J., Wineman, A., 2013. Chemomechanics and homeostasis in active strain stabilized hyperelastic fibrous microstructures. Int. J. Non-Linear Mech. 56, 86–93.
Ezra, D.G., Ellis, J.S., Beaconsfield, M., Collin, R., Bailly, M., 2010. Changes in fibroblast mechanostat set point and mechanosensitivity: an adaptive response to mechanical stress in floppy eyelid syndrome. Investig. Ophthalmol. Vis. Sci. 51, 3853–3863.
Flynn, B.P., Bhole, A.P., Saeidi, N., Liles, M., DiMarzio, C.A., Ruberti, J.W., 2010. Mechanical strain stabilizes reconstituted collagen fibrils against enzymatic degradation by mammalian collagenase matrix metalloproteinase 8 (MMP-8). PLoS One 5.
Foolen, J., van Donkelaar, C.C., Soekhradj-Soechit, S., Ito, K., 2010. European Society of Biomechanics SM Perren Award 2010: an adaptation mechanism for fibrous tissue to sustained shortening. J. Biomech. 43, 3168–3176.
Gyoneva, L., Hovell, C.B., Pewowaruk, R.J., Dorfman, K.D., Segal, Y., Barocas, V.H., 2016. Cell-matrix interaction during strain-dependent remodelling of simulated collagen networks. Interface Focus 6.
Hadi, M.F., Sander, E.A., Ruberti, J.W., Barocas, V.H., 2012. Simulated remodeling of loaded collagen networks via strain-dependent enzymatic degradation and constant-rate fiber growth. Mech. Mater. 44, 72–82.
Heck, T.A.M., Wilson, W., Foolen, J., Cilingir, A.C., Ito, K., van Donkelaar, C.C., 2015. A tissue adaptation model based on strain-dependent collagen degradation and contact-guided cell traction. J. Biomech. 48, 823–831.
Huang, C., Yannas, I.V., 1977. Mechanochemical studies of enzymatic degradation of insoluble collagen-fibers. J. Biomed. Mater. Res. 11, 137–154.
Humphrey, J.D., Holzapfel, G.A., 2012. Mechanics, mechanobiology, and modeling of human abdominal aorta and aneurysms. J. Biomech. 45, 805–814.
Humphrey, J.D., Rajagopal, K.R., 2002. A constrained mixture model for growth and remodeling of soft tissues. Math. Model. Methods Appl. Sci. 12, 407–430.
Jhun, C.-S., Evans, M.C., Barocas, V.H., Tranquillo, R.T., 2009. Planar biaxial mechanical behavior of bioartificial tissues possessing prescribed fiber alignment. J. Biomech. Eng. Trans. ASME 131.
Kerckhoffs, R.C.P., 2012. Computational modeling of cardiac growth in the post-natal rat with a strain-based growth law. J. Biomech. 45, 865–871.
Li, Q., Muragaki, Y., Hatamura, I., Ueno, H., Ooshima, A., 1998. Stretch-induced collagen synthesis in cultured smooth muscle cells from rabbit aortic media and a possible involvement of angiotensin II and transforming growth factor-beta. J. Vasc. Res. 35, 93–103.
Loerakker, S., Obbink-Huizer, C., Baaijens, F.P.T., 2014. A physically motivated constitutive model for cell-mediated compaction and collagen remodeling in soft tissues. Biomechanics Model. Mechanobiol. 13, 985–1001.
Lubarda, V.A., Hoger, A., 2002. On the mechanics of solids with a growing mass. Int. J. Solids Struct. 39, 4627–4664.
Magnusson, S.P., Langberg, H., Kjaer, M., 2010. The pathogenesis of tendinopathy: balancing the response to loading. Nat. Rev. Rheumatol. 6, 262–268.
Menzel, A., Kuhl, E., 2012. Frontiers in growth and remodeling. Mech. Res. Commun. 42, 1–14.
Miller, B.F., Olesen, J.L., Hansen, M., Dossing, S., Crameri, R.M., Welling, R.J., Langberg, H., Flyvbjerg, A., Kjaer, M., Babraj, J.A., Smith, K., Rennie, M.J., 2005. Coordinated collagen and muscle protein synthesis in human patella tendon and quadriceps muscle after exercise. J. Physiol. London 567, 1021–1033.
Mubyana, K., Corr, D.T., 2018. Cyclic uniaxial tensile strain enhances the mechanical properties of engineered, scaffold-free tendon fibers. Tissue Eng. 24, 1808–1817.
Nguyen, C., Cone, F.E., Nguyen, T.D., Coudrillier, B., Pease, M.E., Steinhart, M.R., Oglesby, E.N., Jefferys, J.L., Quigley, H.A., 2013. Studies of scleral biomechanical behavior related to susceptibility for retinal ganglion cell loss in experimental mouse glaucoma. Investig. Ophthalmol. Vis. Sci. 54, 1767–1780.
Nguyen, T.D., Boyce, B.L., 2011. An inverse finite element method for determining the anisotropic properties of the cornea. Biomechanics Model. Mechanobiol. 10, 323–337.
Nguyen, T.D., Jones, R.E., Boyce, B.L., 2007. Modeling the anisotropic finite-deformation viscoelastic behavior of soft fiber-reinforced composites. Int. J. Solids Struct. 44, 8366–8389.
Pijanka, J.K., Spang, M.T., Sorensen, T., Liu, J., Nguyen, T.D., Quigley, H.A., Boote, C., 2015. Depth-dependent changes in collagen organization in the human peripapillary sclera. PLoS One 10.
Prajapati, R.T., Chavally-Mis, B., Herbage, D., Eastwood, M., Brown, R.A., 2000. Mechanical loading regulates protease production by fibroblasts in three-dimensional collagen substrates. Wound Repair Regen. 8, 226–237.
Rausch, M.K., Dam, A., Goktepe, S., Abilez, O.J., Kuhl, E., 2011. Computational modeling of growth: systemic and pulmonary hypertension in the heart. Biomechanics Model. Mechanobiol. 10, 799–811.
Rodriguez, E.K., Hoger, A., McCulloch, A.D., 1994. Stress-dependent finite growth IN soft elastic tissues. J. Biomech. 27, 455–467.
Ruberti, J.W., Hallab, N.J., 2005. Strain-controlled enzymatic cleavage of collagen in loaded matrix. Biochem. Biophys. Res. Commun. 336, 483–489.
Sander, E.A., Barocas, V.H., Tranquillo, R.T., 2011. Initial fiber alignment pattern alters extracellular matrix synthesis in fibroblast-populated fibrin gel cruciforms and correlates with predicted tension. Ann. Biomed. Eng. 39, 714–729.
Susilo, M.E., Paten, J.A., Sander, E.A., Nguyen, T.D., Ruberti, J.W., 2016. Collagen Network Strengthening Following Cyclic Tensile Loading (Vol 6, 20150088, 2016). Interface Focus 6.
Taber, L.A., 1998. A model for aortic growth based on fluid shear and fiber stresses. J. Biomech. Eng. Trans. ASME 120, 348–354.
Taber, L.A., Humphrey, J.D., 2001. Stress-modulated growth, residual stress, and vascular heterogeneity. J. Biomech. Eng. Trans. ASME 123, 528–535.
Tonge, T.K., Ruberti, J.W., Nguyen, T.D., 2015. Micromechanical modeling study of mechanical inhibition of enzymatic degradation of collagen tissues. Biophys. J. 109, 2689–2700.
Topol, H., Demirkoparan, H., Pence, T.J., Wineman, A., 2014. A theory for deformation dependent evolution of continuous fibre distribution applicable to collagen remodelling. IMA J. Appl. Math. 79, 947–977.
Topol, H., Demirkoparan, H., Pence, T.J., Wineman, A., 2017. Time-evolving collagen-like structural fibers in soft tissues: biaxial loading and spherical inflation. Mech. Time-Dependent Mater. 21, 1–29.
Watton, P.N., Ventikos, Y., Holzapfel, G.A., 2009. Modelling the growth and stabilization of cerebral aneurysms. Math. Med. Biol. J. Ima 26, 133–164.
Wong, M., Siegrist, M., Goodwin, K., 2003. Cyclic tensile strain and cyclic hydrostatic pressure differentially regulate expression of hypertrophic markers in primary chondrocytes. Bone 33, 685–693.
Young, R.D., 1985. The ultrastructural organization of proteoglycans and collagen in human and rabbit scleral matrix. J. Cell Sci. 74, 95–104.
Zareian, R., Church, K.P., Saeidi, N., Flynn, B.P., Beale, J.W., Ruberti, J.W., 2010. Probing collagen/enzyme mechanochemistry in native tissue with dynamic, enzyme-induced creep. Langmuir 26, 9917–9926.